doi:10.3772/j.issn.1006-6748.2019.03.009

Optimal configuration strategy of energy storage system in high photovoltaic penetration micro-grid based on voltage sensitivity analysis①

Ouyang Jing (欧阳静), Pan Guobin②, Chen Jinxin, Chai Fushuai, Zhang Libin
(Key Laboratory of Special Purpose Equipment and Advanced Manufacturing Technology, Ministry of Education & Zhejiang Province, Zhejiang University of Technology, Hangzhou 310014, P. R. China)

Abstract

Energy storage is an effective measure to deal with internal power fluctuation of micro-grid and ensure stable operation, especially in the micro-grid with high photovoltaic (PV) penetration. Its capacity configuration is related to the steady, safety and economy of micro-grid. In order to improve the absorptive capacity of micro-grid on maximizing the use of distributed PV power in micro-grid, and improve the power quality, an optimal energy storage configuration strategy is proposed, which takes many factors into account, such as the topology of micro-grid, the change of irradiance, the load fluctuation and the cable. The strategy can optimize the energy storage allocation model to minimize the storage power capacity and optimize the node configuration. The key electrical nodes are identified by using the sensitivity coefficient of the voltage, and then the model is optimized to simplify calculation. Finally, an example of the European low-voltage micro-grid and a micro-grid system in the laboratory is used to verify the effectiveness of the proposed method. The results show that the proposed method can optimize the allocation of capacity and the node of the energy storage system.

Key words: high photovoltaic (PV) penetration, micro-grid, energy storage configuration, voltage sensitive coefficient

0 Introduction

With the decreasing of distributed energy cost, the proportion of distributed energy in micro-grid is gradually increasing. In the future, photovoltaic (PV) will be the main distributed energy in micro-grid in cities. PV output has characteristics of randomness and intermittence, and is connected to the micro-grid by power electronic interface, which has little inertia and poor anti-interference ability. When the photovoltaic penetration is high, due to the inherent characteristics of photovoltaic power supply, it has a negative impact on voltage stability and safe operation of micro-grid.

The micro-grid is connected to the power grid through a transformer at the point of point of common coupling (PCC), which limits the power delivered to the micro-grid. The power input from PCC is not sufficient to balance the voltage when the PV power is affected by clouds in a short time. The configuration of the energy storage system (ESS) can stabilize the fluctuation of PV output power and improve PV utilization rate, especially in the case of high photovoltaic penetration micro-grid. While ensuring the safety and stable operation of the micro-grid, the storage capacity and the optimal configuration node are of great significance to the power quality of the micro-grid and the consumption of the distributed energy[1-3]. Considering the volume and price of the ESS, it is necessary to study the capacity and optimal node configuration of energy storage in high PV penetration micro-grid.

The application of ESS in the micro-grid includes peak shaving and valley filling, operating reserve and smoothing line power fluctuations[4-6]. In Ref. [7], the spectrum of distributed energy output was analyzed by discrete Fourier transform. It took the operating characteristic of ESS as the constraint, then got the minimum capacity of ESS that meets the demands for smooth output operation. Taking peak shaving and valley filling as optimization objective, and considering the maximum power of charge/discharge and power flow constraint, an optimal allocation model of ESS was

① Supported by the National Program of International S&T Cooperation (No. 2014DFE60020), and Natural Science Foundation of Zhejiang Province (No. LY15E070004).
② To whom correspondence should be addressed. E-mail: gbpan@zjut.edu.cn
Received on July 20, 2018

established and solved by particle swarm optimization (PSO) in Ref. [8], but the location of ESS was not given. In Ref. [9], an energy storage allocation model with minimum annual operation cost as the objective function was established under the constraint of volatility. The capacity allocation model was established with the target of minimum operating cost in Ref. [10]. Some of these methods only consider the optimal economic problem, but ignore the power quality problem caused by distributed energy in micro-grids. Some only consider the capacity of ESS, while ignoring the location.

An optimal configuration model of energy storage systems with high PV penetration micro-grid considering PCC point power constraint is proposed in this paper, and the model is optimized by voltage sensitivity coefficient. The optimal solution of the model is the minimum power capacity and the optimal node configuration scheme of the energy storage device, which makes sure the voltage fluctuation of all nodes in the micro-grid in accordance with the power quality standard. The model takes into account various factors, such as micro-grid topology, line parameters, environmental temperature, irradiance, etc., which can be used to evaluate the acceptance capacity of micro-grid for PV systems. The effectiveness of the proposed method is demonstrated by the European low-voltage micro-grid and micro-grid in laboratory.

1 High photovoltaic penetration micro-grid

1.1 Definition of photovoltaic penetration

At present, there is no uniform definition of PV penetration, the PV penetration in this study is defined as the ratio of total PV power(installed capacity) to actually consumed load power[11], as shown in Eq. (1).

$$\mathrm{PV}_{\mathrm{penetration}} = \frac{\text{PV install capacity (kWh)}}{\text{actual consumed load power (kWh)}} \tag{1}$$

1.2 Influence of PV output fluctuation

PV output is susceptible to environmental factors, such as solar irradiance, temperature, in which the impact of solar radiation is the largest[12]. When the temperature remains constant, the relationship between the PV system output and the solar irradiance can be approximately represented as the following expression[13]:

$$P_{pv}(t) = \begin{cases} \dfrac{P_{sn}R(t)^2}{R_{std}R_c}, & 0 \leqslant R(t) < R_c \\ \dfrac{P_{sn}R(t)}{R_{std}}, & R_c \leqslant R(t) < R_{std} \\ P_{sn}, & R_{std} \leqslant R(t) \end{cases} \tag{2}$$

where $P_{pv}(t)$ is the output power of a PV system at time t (MW), P_{sn} is the rated power of PV system (MW), R_{std} is the unit luminous intensity in the standard environment ($\mathrm{W/m^2}$), R_c is the setting specific luminous intensity values ($\mathrm{W/m^2}$).

When the cloud blocks PV panels, the amplitude and frequency of the voltage in the system will be affected. Within the micro-grid system R/X ratio is much larger than the bulk power system, the fluctuation of PV output is closely related to voltage fluctuation.

The fastest rate of irradiance change can reach 705 $\mathrm{W/m^2}$ per second due to the influence of clouds[14], and the location of the micro-grid is small, so it's a short time for clouds to cover the PV panels. When the penetration exceeds 20%, the fluctuation of PV output caused by clouds can cause voltage fluctuation showed in Ref. [15]. As shown in Ref. [16], when the PV penetration reaches 30% and clouds cover 20 s in PV panels, the voltage of a node within the system is reduced to 0.891 pu for up to 15 s. If there is no effective measure to be taken during this period, it is possible that PV inverters will be out of the system[17], and cause more serious problems. Another effect is that when the load in the micro-grid is small, and the output of PV systems is relatively large, terminal voltage will rise[18]. In this case, it is necessary to use ESS to achieve the purpose of dynamic power balancing in micro-grid.

2 Energy storage system configuration model

2.1 The objective function

Considering the investment and operation cost of the energy storage system, the optimal allocation objective is to minimize the sum of the storage power capacity of the configurable nodes. The corresponding model objective function is

$$S = \min \sum_{n=1}^{N} \sqrt{(P_{s,n}^2 + Q_{s,n}^2)} \tag{3}$$

where S is the sum of the power capacity of the energy storage system, N is the total number of electrical nodes in the micro-grid system, $P_{s,n}$ and $Q_{s,n}$ are the active and reactive capacities of the energy storage system on node n.

2.2 Constraint conditions of system safety operation

In the energy storage optimization strategy of high photovoltaic penetration micro-grid, the capacity of the PV system and the ESS, the balance of the micro-grid-

power flow and the voltage are taken into account.

2.2.1 PV system output constraints

The output of the PV system is closely related to factors such as installed capacity of PV, irradiance, ambient temperature and conversion efficiency. It is difficult to realize the peak power of the PV system due to the ambient temperature and the solar irradiance.

$$P_{PV,n} = P_{zhuangji,n} FT\eta \tag{4}$$

$$0 \leqslant P_{PV,n} \leqslant P_{zhuangji,n} \tag{5}$$

$$0 \leqslant Q_{PV,n} \leqslant Q_{pv\max,n} \tag{6}$$

where $P_{zhuangji,n}$ is the installed capacity of the PV system at node n, $Q_{pv\max,n}$ is the reactive output limit of the PV system at node n, F is the irradiance, T is the ambient temperature, η is the conversion efficiency, $P_{PV,n}$ is the actual active power output of PV system at node n, $Q_{PV,n}$ is the actual reactive power output of PV system at node n.

2.2.2 ESS power constraints

The energy absorbed or released by ESS shall not exceed the upper limit of its power capacity configuration.

$$-S_B^{\max} \leqslant \mu_n \sqrt{P_{s,n}^2 + Q_{s,n}^2} \leqslant S_B^{\max} \tag{7}$$

where μ_n is the 0 – 1 variable, $P_{s,n}$ and $Q_{s,n}$ are the active and reactive capacities of the energy storage system at node n, $S_B^{\max}$ is the maximum power of the preset ESS, when it is positive, it means to discharge, and when negative it means to charge.

2.2.3 Power flow balancing and voltage constraints in micro-grid systems

In order to ensure the stable operation of the micro-grid system, the active and reactive power balance of the system must be satisfied, and the voltage at each node in the system is within the limits of the power quality standard. Eqs(8) and (9) are static power flow constraint equations of micro-grid.

$$P_{PV,n} + P_{S,n} - P_{L,n} = U_n \sum_{k=1}^{N} U_k (G_{nk}\cos\theta_{nk} + B_{nk}\sin\theta_{nk}) \tag{8}$$

$$Q_{PV,n} + Q_{S,n} - Q_{L,n} = U_n \sum_{k=1}^{N} U_k (G_{nk}\sin\theta_{nk} - B_{nk}\cos\theta_{nk}) \tag{9}$$

$$U_{\min} \leqslant U_n \leqslant U_{\max} \tag{10}$$

where $P_{PV,n}$ and $Q_{PV,n}$ represent the active and reactive power outputs of PV system at node n respectively, U and θ represent the amplitude and phase angle of node voltage respectively, G and B are the conductance and the susceptance of the corresponding branch, the subscript n, k is the corresponding electrical node number. In Eq.(10), $U_{\min}$ and $U_{\max}$ are the voltage limits of nodes in the micro-grid system.

2.2.4 Power flow constraint at PCC

The micro-grid is connected to the bulk power system through the PCC, and the capacity of the transformer at PCC determines the power flow between the micro-grid and the bulk power system. When the power flow at PCC does not reach the rated capacity of the transformer, the PCC point can be treated as a balanced node. When meteorological factors such as irradiance mutation or insert high-power impact loads, the power flow at PCC reaches the rated capacity of the transformer. PCC should be regarded as a PV bus in power flow calculation. The power flow of PCC should not exceed the rated capacity of the transformer, and Eq.(11) needs to be satisfied:

$$-S_{trans} \leqslant \sqrt{P_{PCC}^2 + Q_{PCC}^2} \leqslant S_{trans} \tag{11}$$

where P_{PCC} and Q_{PCC} are active and reactive powers of PCC respectively, when it is positive, it means that the power is absorbed from the bulk power system, and if it is negative, it means the energy is fed into the bulk power system from the micro-grid. S_{trans} is the rated capacity of the transformer at PCC.

2.2.5 Power flow constraint of branch

In order to ensure the safe and stable operation of the micro-grid system, variation range of the branch flow should be limited to the range of the line transmission capacity.

$$-F_{b,n} \leqslant f_{b,n} \leqslant F_{b,n} \tag{12}$$

where $f_{b,n}$ is the power flow of the branch bus n, $F_{b,n}$ is the maximum power flow value of branch bus n.

3 Model optimization and solution

3.1 Identification of key nodes

Most of the sensitivity analyses in voltage stability analyses are based on the power flow equation which is based on node power balance. The system power flow equation considering the resistance and inductance characteristics of the power line is as follows[19]:

$$P_i = \sum_{k=1}^{N} |U_i||U_j||Y_{ij}|\cos(\theta_{ij} - \delta_i + \delta_j) \tag{13}$$

$$Q_i = \sum_{k=1}^{N} |U_i||U_j||Y_{ij}|\sin(\theta_{ij} - \delta_i + \delta_j) \tag{14}$$

where, P_i and Q_i represent the active and reactive power at node i respectively; U_i and U_j represent the voltage amplitude at nodes i and j, respectively; δ_i and δ_j represent the voltage phase angle at nodes i and j; $Y_{ij} < \theta_{ij}$ is the admittance of line between nodes i and j.

The sensitivity of the node voltage to active and reactive deviations can be calculated by the Newton-Raphson method for Eq.(13) and Eq.(14).

$$\begin{vmatrix} \Delta P \\ \Delta Q \end{vmatrix} = \begin{vmatrix} \partial P/\partial \delta & \partial P/\partial U \\ \partial Q/\partial \delta & \partial Q/\partial U \end{vmatrix} \cdot \begin{vmatrix} \Delta \delta \\ \Delta U \end{vmatrix} \quad (15)$$

Eq. (16) can be obtained by Eq. (15):

$$\begin{vmatrix} \Delta \delta \\ \Delta U \end{vmatrix} = \begin{vmatrix} S_{\delta P} & S_{\delta q} \\ S_{up} & S_{uq} \end{vmatrix} \cdot \begin{vmatrix} \Delta P \\ \Delta Q \end{vmatrix} \quad (16)$$

In each iteration, the Jacobian matrix of the system is updated until the convergence condition is satisfied, then the voltage sensitivity matrix is obtained by the inverse Jacobi matrix.

The 5-node low-voltage micro-grid system is shown in Fig. 1. When the 10 kW active power is injected into the nodes 1 – 4 respectively, the voltage sensitivity analysis is carried out to analyze the influence of the same power on the voltage of each node in the micro-grid. In order to facilitate the analysis, it is assumed that the three-phase power flow is balancing, and the load is 0.

Parameters of the micro-grid system are as follows (the unit of impedance is Ω/km): the transformer at PCC, 20 kV/0.4 kV, Dyn11, 50 Hz, 400 kVA, $u_k\% = 4\%$, $r_k\% = 1\%$; the type of the line is 4×25 mm^2Cu, $R_{ph} = 0.871$, $X_{ph} = 0.081$. The length of the line between two nodes is 150 m.

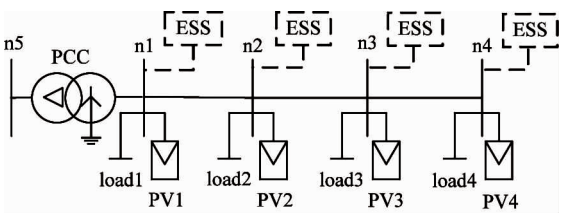

Fig. 1 The topology of a 5-node micro-grid system

The test parameters for the 5-node micro-grid system are shown in Table 1. The voltage sensitivity coefficient matrix is calculated by using Eqs(13) – (16), and the sensitivity coefficient of voltage amplitude and active power, the sensitivity coefficient of voltage amplitude and reactive power are obtained, as shown in Table 2 and Table 3, respectively, where $S_{up}(4,4)$ is 2.1247 pu/MW, which indicates that 10 kW of active power is injected into node 4 and the voltage at node 5 rises by 4.91 V.

Table 1 The test parameters for the 5-node micro-grid system

Base voltage	0.4 kV
Base power	1 MVA
Slack bus voltage	1.02 pu
Cable impedance per segment	0.8166 + j0.07596 pu
Transformer impedance	0.0625 + j0.1

It can be seen from Table 2 that the same capacity of the power is injected at different nodes, and the support of node 4 in the micro-grid system is more effective. Based on this characteristic, the voltage sensitivity coefficient can be used to configure active and reactive power to different nodes in micro-grid, to achieve the purpose of using the minimum power to achieve the voltage support.

Table 2 Sensitivity coefficient of voltage amplitude and active power(pu/MW)

S_{up}	1	2	3	4
1	0.0593	0.0564	0.0545	0.0536
2	0.0568	0.7851	0.7623	0.7513
3	0.0552	0.7628	1.4559	1.4349
4	0.0544	0.7519	1.4352	2.1247

Table 3 Sensitivity coefficient of voltage magnitude and reactive power(pu/MW)

S_{uq}	1	2	3	4
1	0.0957	0.0957	0.0957	0.0957
2	0.0916	0.1612	0.1612	0.1612
3	0.0890	0.1566	0.2242	0.2242
4	0.0877	0.1544	0.2210	0.2875

3.2 Model optimization

The length of cables within the micro-grid is relatively short, compared with the bulk power system, the R\X ratio is high, and the base voltage is low, so the impedance of the line has influence on the voltage amplitude. In this paper, the active and reactive sensitivity of the voltage amplitude is used to optimize the model.

From Eq. (16), it can be concluded that the effect of active and reactive power fluctuations of node j on the voltage amplitude of node i is

$$\Delta U_i = S_{up}(i,j) \cdot \Delta P_j + S_{uq}(i,j) \cdot \Delta Q_j \quad (17)$$

where $S_{up}(i,j)$ and $S_{uq}(i,j)$ are the sensitivity of active and reactive power fluctuations at node j to the voltage amplitude of node i, ΔP_j and ΔQ_j are the active and reactive fluctuation values at node j respectively, ΔU_i is the fluctuation value of the voltage amplitude at node i.

Combining Eq. (8) and Eq. (9) the voltage amplitude at node n can be expressed as

$$U_n = U_G + \sum_{k=1}^{N} S_{up}(n,k)(P_{PV,k} + P_{s,k} - P_{L,k}) + \sum_{k=1}^{N} S_{uq}(n,k)(Q_{PV,k} + Q_{s,k} - Q_{L,k}) \quad (18)$$

where U_G is the voltage of the bulk power system at PCC, $P_{PV,k}$ and $Q_{PV,k}$ represent the active and reactive power output of PV system at node k respectively, $P_{s,k}$

and $Q_{s,k}$ represent the active and reactive power output of the energy storage system at node k respectively, $P_{L,k}$ and $Q_{L,k}$ represent the active and reactive power consumed by the load at node k respectively. All voltage and power are converted to the value per unit when the voltage sensitivity coefficient is obtained. In order to keep consistent, all the data mentioned above are also normalized.

In order to convert as much sunlight energy as possible, PV inverters are generally required to operate in a state close to the unit power factor. PV systems in the model can only consider the active power, and the reactive power is 0. The reactive power in micro-grid is mainly provided by the bulk power system and ESS.

It can be seen that the ESS configuration model is a combination problem for the power allocation in PV systems, energy storage system and load. The objective function and constraint condition are linear and a mixed integer linear programming model which can be solved by linear programming. CPLEX optimization software package or Yalmip toolbox in Matlab can solve the above model. The optimal solution of the model is the minimum capacity and the optimal node configuration to meet the stability of the high photovoltaic penetration micro-grid.

4 Experiment and demonstration

4.1 Verification in EU low-voltage micro-grid

In order to study the ESS of high PVpenetration micro-grid when the PV output fluctuation or load impact occurs, this section takes the typical low-voltage micro-grid topology proposed in the European (EU) micro-grid research project[20] as an example. The energy storage configuration strategy of the short-time voltage amplitude decline caused by the induction motor is tested when the PV output fluctuates.

Nodes in this topology are renumbered as shown in Fig. 2. The corresponding relationship between the nodes is that node 3 in Fig. 2 corresponds to load 1 in the original topology, node 6 corresponds to load 2, node 8 corresponds to load 3, node 10 corresponds to load 4, and node 11 corresponds to load 5.

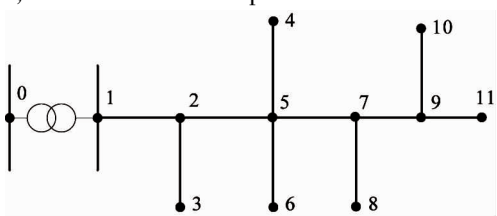

Fig. 2 EU low-voltage micro-grid topology

Scenario 1: PV penetration is 40%. The EU low-voltage micro-grid system test parameters are as follows: the base voltage is 0.4 kV, the base power is 1 MVA and the slack bus voltage is 1.05 pu. The type, capacity, node location of DG sources and loads are shown in Table 4 and Table 5, respectively.

When parts of the PV panels are covered by clouds, PV output dropped to 75%, a 120 kW induction motor is accessed at node 7. The motor's power factor is 0.75, the starting current is 6 times of the rated current. The active power consumed by the motor is 120 kW and the reactive power is 180 kVar during the full load starting process. The proposed method is used to configure the ESS to achieve the goal that the voltage amplitude of all nodes is no less than 0.9 times the base voltage.

Table 4 The type, capacity, and node location of DG sources

Node	The type of DG sources	Active power (kW)	Reactive power (kVar)
4	Photovoltaic(pq)	40	4.4
6	Photovoltaic(pq)	20	2.2
11	Wind power generation (pv)	40	Max 5.5 Min 3.3

Table 5 The capacity, and location of loads

Node	Active power (kW)	Reactive power (kVar)
3	40	4
5	50	0
8	30	0
9	60	6
10	30	1.5

The active power voltage sensitivity coefficient and the reactive power voltage sensitivity coefficient in scenario 1 can be found in the Appendix. The optimal configuration node in scenario 1 is node 8, the configuration active power is 22.25 kW, and the reactive power is 6.89 kVar.

To prove the accuracy of the proposed method, the capacity required for ESS in a single node in scenario 1

is shown in Table 6. It can be seen that the minimum capacity required for energy storage is at node 8.

Table 6 Energy storage configuration capacity of each node

Node	Active power (kW)	Reactive power (kVar)
1	62.3468	95.7592
2	54.4155	28.8903
3	51.7451	25.7976
4	42.8157	19.9354
5	42.4574	19.5137
6	43.4247	20.5304
7	30.0505	12.1781
8	22.2535	6.8880
9	30.0293	12.1495
10	31.2790	13.1420
11	30.6387	12.6301

The minimum capacity required to configure energy storage at multiple nodes in scenario 1 is shown in Table 7. It can be seen that the minimum capacity required for energy storage is at node 8.

In order to verify the effect of energy storage configuration, the power flow distribution in scenario 1 with no energy storage configuration and the corresponding energy storage capacity at node 8 in accordance with the calculation results is calculated respectively. The voltage fluctuation before and after energy storage configuration in scenario 1 is shown in Fig. 3. It can be seen that the node voltage has improved significantly and the voltage amplitude is above 0.9 pu after the configuration, which demonstrates the effectiveness of the proposed method.

Table 7 Minimum capacity of multi nodes energy storage configuration (Scenario 1)

Total Number		1	2	3	4	5	6	7	8	9	10	11
1	AP(kW)	-	-	-	-	-	-	-	22.2535	-	-	-
	RP(kVar)	-	-	-	-	-	-	-	6.8880	-	-	-
2	AP(kW)	-	-	-	-	-	-	-	14.6675	10.2353	-	-
	RP(kVar)	-	-	-	-	-	-	-	4.1431	4.5399	-	-
3	AP(kW)	-	-	-	-	-	-	7.6285	10.9446	7.6374	-	-
	RP(kVar)	-	-	-	-	-	-	3.0915	3.3876	3.0900	-	-
4	AP(kW)	-	-	-	-	-	-	6.1371	8.8049	6.1443	-	5.9899
	RP(kVar)	-	-	-	-	-	-	2.4871	2.7253	2.4859	-	2.4692

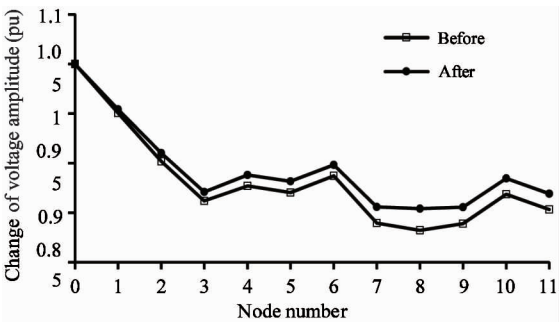

Fig. 3 Voltage distribution of each node before and after energy storage

4.2 Verification of energy storage configuration in laboratory micro-grid

In order to verify the feasibility of the proposed energy storage configuration method, the micro-grid of the laboratory is used for verification which is connected to the bulk power system through the Simulation Grid (California Instruments RS Series), and the topology of the system is shown in Fig. 4.

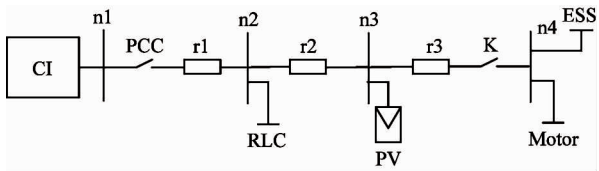

Fig. 4 The topology of the micro-grid of the laboratory

The PCC is defined as node 1, the capacity is 50 KVA; the RLC programmable load is node 2, and the active power is 20 kW; node 3 is PV, and the output active power is 7.5 kW; the induction motor is node 4, the rated power is 5.5 kW. The base voltage is 0.4 kV, the base power is 1 MVA, and the voltage of the bulk power system at PCC is 1.05 pu.

The line analog impedance is connected between

two nodes. The analog line length between node 1 and node 2 is 350 m and impedance $r1$ is 0.1 + j0.029 Ω. The analog line length between node 2 and node 3 is 350 m, and the impedance $r2$ is the same as $r1$. The analog line length between node 3 and node 4 is 750 m and impedance $r3$ is 0.22 + j0.0672Ω.

When the system is stable, close the circuit breaker K, and the 5.5 kW induction motor is connected to the system with a full load. The voltage amplitude of node 4 is pulled down to 0.96 pu, then make the voltage amplitude of the node 4 not less than 1.0 pu through the energy storage configuration.

According to the proposed method, the active and reactive sensitivity coefficients of voltage amplitude is shown in Table 8 and Table 9, respectively. The optimal node for the energy storage configuration is node 4, the minimum capacity of active power is 2.97 kW, and reactive power is 1.3267 kVar. Considering the need of practical engineering, the final energy storage configuration results are retained 1 decimal place, the active power is 3.0 kW, and reactive power is 1.3 kVar, respectively.

Table 8 Sensitivity coefficient of voltage amplitude and active power(pu/MW)

S_{up}	1	2	3	4
1	0.1463	0.1826	0.1617	0.1617
2	0.1557	2.6963	2.5811	2.5811
3	0.1503	2.6037	4.7828	4.7828
4	0.1503	2.6037	4.7828	9.9175

Table 9 Sensitivity coefficient of voltage amplitude and reactive power(pu/MW)

S_{uq}	1	2	3	4
1	1.4586	1.4591	1.4592	1.4592
2	1.5519	2.255	2.2556	2.2556
3	1.4986	2.1775	2.8552	2.8552
4	1.4986	2.1775	2.8552	4.4236

When the 5.5 kW induction motor is connected to the system with a full load, the active power of 3.1 kW is injected into node 4. The voltage amplitude fluctuation of node 4 is recorded by the Fluke435 power quality analyzer, as shown in Fig. 5, and the sampling interval is 0.5 s. It can be seen that the voltage amplitude of node 4 rises from 212.4 V to 220.2 V, which is in accordance with the experimental expectations. The experimental results show that the proposed method of energy storage configuration is feasible.

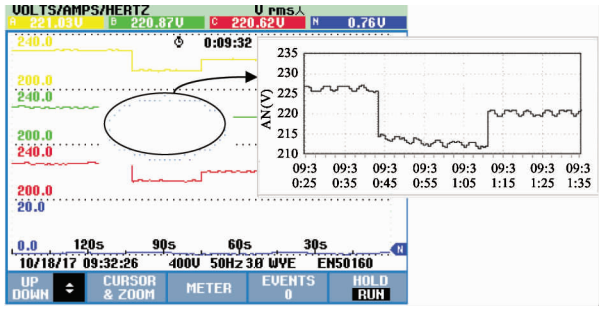

Fig. 5 The voltage amplitude of node 4

5 Conclusions

In this paper, an optimized configuration model of high photovoltaic penetration micro-grid energy storage system is proposed, and the model is optimized by voltage sensitivity coefficient. The optimal solution of the model is to satisfy the minimum power capacity and optimal node configuration of the energy storage device, which meets the voltage fluctuation of all nodes in the micro-grid in accordance with the national power quality standard. Experiments are carried out both in micro-grid model based on the European low-voltage micro-grid topology and a micro-grid system built in the laboratory. The results show that the proposed method can effectively suppress the power fluctuation and stabilize the voltage in micro-grid.

References

[1] Bie Z H, Li G F, Xie H P. Reliability evaluation of microgrids considering coordinative optimization of loads and storage devices[J]. *Transactions of China Electrotechnical Society*, 2014(2): 64-73

[2] Xiao J, Zhang Z Q, Zhang P, et al. A capacity optimization method of hybrid energy storage system for optimizing tie-line power in microgrids[J]. *Automation of Electric Power System*, 2014(12): 19-26

[3] Morstyn T, Hredzak B, Agelidis V G. Control strategies for microgrids with distributed energy storage systems: an overview[J]. *IEEE Transactions on Smart Grid*, 2018, 9(4):3652-3666

[4] Wang C S, Yu B, Xiao J, et al. An energy storage capacity optimization method for microgrid tie-line power flow stabilization[J]. *Automation of Electric Power System*, 2013(3):12-17

[5] Wang Y, Xiao X Y, Liu Y, et al. Classifying features selection and classification based on mahalanobis distance for complex short time power quality disturbances[J]. *Power System Technology*, 2014(4): 1064-1069

[6] Kang J, Wang S W, Yan C C. A new distributed energy system configuration for cooling dominated districts and the performance assessment based on real site measurements[J]. *Renewable Energy*, 2019, 131: 390-403

[7] Wu J, Ding M, Zhang J J. Capacity configuration method of energy storage system for wind farm based on cloud model and K-means clustering[J]. *Automation of Electric Power Systems*, 2018, 42(24):67-76
[8] Yang Y Q, Niu L Y, Tian L T, et al. Configuration of energy storage devices in regional distribution network considering optimal load control[J]. *Power System Technology*, 2015(4):1019-1025
[9] Lu J L, Yang Y, Wang Y, et al. Copula-based capacity configuration of energy storage system for a PV-assisted electric vehicles charging station[J]. *Acta Energiae Solaris Sinica*, 2016(3):780-786
[10] Tang J, Li X R, Huang J Y, et al. Capacity allocation of BESS in secondary frequency regulation with the goal of maximum net benefit[J]. *Transactions of China Electrotechnical Society*, 2019, 34(5):963-972
[11] Pourmousavi S A, Cifala A S, Nehrir M H. Impact of high penetration of PV generation on frequency and voltage in a distribution feeder[C]. In: Proceedings of the 2012 North American Power Symposium (NAPS), Champaign, USA, 2012. 1-8
[12] Cai S B, Tong J J, Bao G J, et al. Convex decomposition of concave clouds for the ultra-short-term power prediction of distributed photovoltaic system[J]. *High Technology Letters*, 2016, 22(3): 305-312
[13] Wang M, Zong X J, Yuan Y, et al. Reliability analysis of generation systems with photovoltaic stations[J]. *Proceedings of the CSEE*, 2013(34): 42-49
[14] Tomson T. Fast dynamic processes of solar radiation[J]. *Solar Energy*, 2010(84): 318-323
[15] Mc Granaghan M, Ortmeyer T, Crudele D, et al. Advanced grid planning and operations, NREL/SR-581-42294/SAND2008-0944[R]. California: Sandia National Laboratories, 2008
[16] Yan R F, Saha T K. Investigation of voltage stability for residential customers due to high photovoltaic penetrations [J]. *IEEE Transactions on Power Systems*, 2012, 27(2): 651-662
[17] China Electricity Council. GB/T 19964-2012 technical requirements for connecting photovoltaic power sataion to power system[S]. Beijing: National Standards of People's Republic of China, 2012
[18] Delfanti M, Merlo M, Pozzi M, et al. Power flows in the Italian distribution electric system with dispersed Generation[C]. In: CIRED 2009-20th International Conference and Exhibition on Electricity Distribution-Part 1, Prague, Czech, 2009. 1-5
[19] Han Z X. Power System Analysis[M]. Third Edition. Hangzhou: Zhejiang University Press. 2005
[20] Esram T, Chapman P L. Comparison of photovoltaic array maximum power point tracking techniques[J]. *IEEE Transactions on Energy Conversion*, 2007, 22(2): 439-499

Ouyang Jing, born in 1984. She received the Ph. D. degree from the College of Mechanical Engineering, Zhejiang University of Technology, Hangzhou, China, in 2017. She is a postdoctoral fellow at Zhejiang University of Technology. Her main research interests are distributed renewable energy, micro-grid and automation of electric power systems.

Appendix

The active power voltage sensitivity coefficient and the reactive power voltage sensitivity coefficient in scenario 1 are given in Table 10 and Table 11.

Table 10 The active power voltage sensitivity coefficient of scene 1(pu/MW)

Node	1	2	3	4	5	6	7	8	9	10	11
1	0.0788	0.0826	0.0893	0.0845	0.0858	0.0826	0.0857	0.087	0.0859	0.0814	0.0835
2	0.0824	0.2474	0.2671	0.252	0.2553	0.2471	0.255	0.2585	0.2553	0.2424	0.2488
3	0.0889	0.2669	1.2681	0.2718	0.2754	0.2665	0.2751	0.2788	0.2754	0.2615	0.2684
4	0.0837	0.2514	0.2713	0.3365	0.3409	0.33	0.3405	0.3452	0.3409	0.3237	0.3323
5	0.0848	0.2544	0.2746	0.3406	0.4671	0.3341	0.3447	0.3494	0.3451	0.3277	0.3364
6	0.0822	0.2468	0.2664	0.3304	0.3347	0.9243	0.3343	0.3388	0.3347	0.3178	0.3263
7	0.0846	0.254	0.2742	0.3401	0.3445	0.3335	0.5064	0.5132	0.507	0.4814	0.4942
8	0.0857	0.2573	0.2778	0.3445	0.349	0.3378	0.513	0.736	0.5136	0.4877	0.5007
9	0.0847	0.2543	0.2745	0.3404	0.3449	0.3339	0.5069	0.5137	0.7497	0.712	0.731
10	0.0805	0.2415	0.2607	0.3234	0.3276	0.3171	0.4815	0.488	0.7122	1.5081	0.6944
11	0.0826	0.2481	0.2678	0.3321	0.3365	0.3257	0.4945	0.5012	0.7315	0.6946	1.1147

Table 11 The reactive power voltage sensitivity coefficient of scene 1 (pu/MW)

Node	1	2	3	4	5	6	7	8	9	10	11
1	0.1215	0.1216	0.1222	0.1216	0.1216	0.1214	0.1216	0.1216	0.1216	0.1211	0.1213
2	0.1271	0.1319	0.1338	0.1319	0.1319	0.1314	0.1319	0.1319	0.1319	0.1304	0.1311
3	0.1371	0.1423	0.1719	0.1423	0.1423	0.1418	0.1423	0.1423	0.1422	0.1407	0.1415
4	0.1291	0.134	0.1359	0.1573	0.1574	0.1567	0.1573	0.1573	0.1573	0.1554	0.1563
5	0.1307	0.1356	0.1376	0.1593	0.1802	0.1586	0.1592	0.1593	0.1592	0.1572	0.1582
6	0.1268	0.1315	0.1334	0.1545	0.1545	0.2427	0.1545	0.1545	0.1544	0.1525	0.1535
7	0.1305	0.1354	0.1374	0.159	0.159	0.1584	0.2061	0.2061	0.2061	0.2032	0.2047
8	0.1322	0.1372	0.1391	0.1611	0.1611	0.1604	0.2088	0.2288	0.2087	0.2058	0.2073
9	0.1306	0.1355	0.1375	0.1592	0.1592	0.1585	0.2063	0.2063	0.277	0.2728	0.275
10	0.1241	0.1288	0.1306	0.1512	0.1512	0.1506	0.196	0.196	0.2632	0.2785	0.2612
11	0.1274	0.1322	0.1342	0.1553	0.1553	0.1547	0.2013	0.2013	0.2703	0.2661	0.3102